Journal of Atmospheric and Solar–Terrestrial Physics 217 (2021) 105531

Contents lists available at ScienceDirect

Journal of Atmospheric and Solar-Terrestrial Physics

journal homepage: www.elsevier.com/locate/jastp

High-latitude polar pattern of ionospheric electron density: Scaling features and IMF dependence

G. Consolini [a,*], R. Tozzi [b], P. De Michelis [b], I. Coco [b], F. Giannattasio [b], M. Pezzopane [b], M. F. Marcucci [a], G. Balasis [c]

[a] INAF-Istituto di Astrofisica e Planetologia Spaziali, Roma, Italy
[b] Istituto Nazionale di Geofisica e Vulcanologia, Roma, Italy
[c] Institute for Astronomy, Astrophysics, Space Applications and Remote Sensing, National Observatory of Athens, Metaxa and Vas. Pavlou St., Penteli, 15236, Athens, Greece

ARTICLE INFO

Keywords:
Polar ionosphere
Turbulence
Scaling feature
Space weather
Swarm satellite
Electron density

ABSTRACT

We investigated the average polar patterns of ionospheric electron density and the corresponding patterns of scaling features as a function of interplanetary magnetic field orientation. The focus is on the Northern Hemisphere using electron density data recorded on-board ESA Swarm A satellite. The first- and second-order scaling exponents have been evaluated by means of the q^{th}-order structure functions. We used electron density measurements over a period of 15 months from April 1, 2014 to June 30, 2015, which corresponds to the maximum of solar cycle 24 and which is characterized by an average value of the solar radio flux (F10.7) index equal to (140 ± 30) sfu. Electron density, first- and second-order scaling exponents have been mapped and discussed for four main IMF orientations provided by B_y and B_z components under conditions of high solar activity. Large spatial changes of the second-order scaling exponent pattern are observed with a steepening of the associated spectral exponent in correspondence with the nightside polar cap trailing edge. Intermittency, defined as the departure from linearity of the dependence of scaling exponents on moment order q, is also evaluated finding that it is generally higher near the equatorward boundary of the auroral oval than elsewhere. On the whole, the found patterns of the electron density first- and second-order scaling exponents suggest the occurrence of turbulence at the high latitudes.

1. Introduction

Changes of the interplanetary conditions both in terms of interplanetary magnetic field (IMF) orientation and solar wind parameters (plasma density, velocity, etc.) deeply influence the circumterrestrial environment, i.e. the Earth's magnetosphere and ionosphere. In particular, changes in IMF orientation are known to be responsible for changes in plasma circulation inside the Earth's magnetosphere-ionosphere system due to the occurrence of magnetic reconnection at the magnetopause (Dungey, 1961). It is well-known and documented in several papers (see e.g., Heppner and Maynard, 1987; Cowley, 1982) that the occurrence of magnetic reconnection process at the low-latitude dayside magnetopause during periods of southward IMF strongly affects plasma circulation in the polar regions causing the formation of two large-scale convection cells (Ruohoniemi and Greenwald, 1996; Cousins and Shepherd, 2010), which transport the plasma from the dayside region to the nightside one through the polar cap. At the same time, the enhancement of the high-latitude current systems, both parallel and perpendicular to the geomagnetic field (field-aligned currents, and auroral electrojets, respectively), provides an increase of plasma deposition in the auroral oval regions and a thermospheric heating via the Joule effect.

One of the possible consequences of these large-scale plasma motions and particle precipitation is the generation of turbulence, both fluid and magnetohydrodynamic, at small and meso-scales (i.e. ranging from a few kilometers up to hundreds of kilometers) due to the triggering of fluid and plasma instabilities, both linear and nonlinear. Turbulence is a very important physical phenomenon, widely studied in literature, that

* Corresponding author.
E-mail addresses: giuseppe.consolini@inaf.it (G. Consolini), roberta.tozzi@ingv.it (R. Tozzi), paola.demichelis@ingv.it (P. De Michelis), igino.coco@ingv.it (I. Coco), fabio.giannattasio@ingv.it (F. Giannattasio), michael.pezzopane@ingv.it (M. Pezzopane), federica.marcucci@inaf.it (M.F. Marcucci), gbalasis@noa.gr (G. Balasis).

https://doi.org/10.1016/j.jastp.2020.105531
Received 30 May 2020; Received in revised form 29 November 2020; Accepted 23 December 2020
Available online 7 January 2021

may play a crucial role in plasma transport and thermospheric heating (see, e.g., Weimer, 2005; Vasyliūnas and Song, 2005; Liu et al., 2018). In the framework of ionospheric phenomena, turbulence, in particular electrostatic turbulence, can involve a large range of time and spatial scales (Dyrud et al., 2008). The interaction of these scales with each other ends up with the generation of increasingly small-scale plasma density irregularities. This has been suggested, for instance, by Basu et al. (1984, 1988); Earle et al. (1989); Giannattasio et al. (2019), who essentially characterized the equatorial and polar regions. These irregularities can deeply influence the propagation of electromagnetic signals in the ionosphere significantly reducing the quality and performance of radio waves and satellite communications, namely the global navigation satellite systems (GNSS) and the global positioning system (GPS).

As discussed in Kintner and Seyler (1985) and Pécseli (2015), in the polar ionosphere the nature of the expected turbulence is mainly related to electrostatic fluctuations and manifests in a turbulent drift velocity field. The investigation of such turbulent medium can be done by investigating the scale-invariant character and the spectral features of the electric field fluctuations or, as an alternative, of the electron density fluctuations. The latter are expected to respond to the drift velocity field as a passive scalar quantity (Consolini et al., 2020a).

Most of the processes responsible for the changes at high latitudes of the ionospheric electron density pattern are driven and/or triggered by the IMF and plasma conditions. A careful investigation of the electron density pattern, its scaling features and their dependence on the interplanetary conditions may provide useful insights in understanding and modeling the solar wind-magnetosphere-ionosphere coupling. In this framework, significant advances in the knowledge of such complex coupling can be produced by the observations on-board polar low Earth orbit satellites, as the European Space Agency (ESA) constellation of Swarm satellites.

Swarm is a minisatellite constellation mission launched in November 2013 by ESA. It consists of three identical satellites flying on two different nearly polar orbital planes at two different altitudes. Two satellites (Swarm A and Swarm C) fly side-by-side at a mean altitude of $\sim$ 450 km (at the present time) at 87.35° inclination angle, the third satellite (Swarm B) orbits at an altitude of $\sim$ 500 km (at the present time) at 87.75° inclination angle (Friis-Christensen et al., 2006, 2008; Knudsen et al., 2003).

The Swarm mission was designed mainly to provide the first global representation of the geomagnetic field and its temporal evolution on different time scales, from a hour to several years, and gain also new insights into the magnetization of the crust and uppermost mantle. However, its orbital features and the instrumentation on-board have attracted also the attention of the scientific community interested in the Sun-Earth interaction. The different parameters measured on-board these satellites have provided, and still provide, the opportunity to improve our knowledge on the electric current systems flowing in the magnetosphere and ionosphere, as well as to investigate the ionospheric plasma dynamics and structure, among others.

In recent years, there has been an increasing amount of literature on different and intriguing aspects of the ionosphere at Swarm altitude: from the survey of the polar cap patches and plasma structuring (Spicher et al., 2015) to a statistical study of ionospheric plasma irregularities at high latitudes (Jin et al., 2019; De Michelis et al., 2020); from the confirmation of the existence of the small-scale field-aligned currents at mid and low latitudes (Iyemori et al., 2015) to the fractal structure of the magnetic field fluctuations associated with the high-latitude field-aligned currents (FACs) (Consolini et al., 2020b); from the study of the scaling features of the geomagnetic field fluctuations to characterize the different ionospheric turbulence regimes at high latitudes (De Michelis et al., 2015, 2016, 2017, 2019, 2020) to the study of small-scale magnetic fluctuations at low and mid latitudes (Yin et al., 2019). These studies have allowed reaching significant progresses in the comprehension of the circumterrestrial environment conditions thanks to a better understanding of the ionospheric dynamics and main structures under different conditions of the geomagnetic disturbance (Materassi et al., 2020). The early studies could not benefit of the large amount of data now available, so they mostly considered case studies that took advantage of the peculiar configuration of the three satellites. However, some studies attempted to approach to the changes of the physical conditions in terms of ion density and velocity field patterns by a statistical point of view (Kivanç and Heelis, 1998). For instance, Kivanç and Heelis (1998) showed that the spatial pattern of irregularities in the high-latitude ionospheric *F* region depends on the external IMF conditions (mainly the direction), the local plasma structures and the conductivity of the underlying ionosphere. Now, six years after the launch of the mission and the collection of loads of data, robust statistical studies are also possible allowing, thus, the possibility of extending previous works to a larger dataset. Unfortunately, most of the time interval covered, so far, by Swarm satellites data is characterized by a low level of solar activity having the satellites been launched when solar cycle 24 was reaching its maximum. So, since the purpose of this work is to carry out a statistical study of the features of electron density fluctuations in the high-latitude Northern ionosphere for different IMF orientations under conditions of high solar activity only, we use data recorded by the Langmuir probe instrument on-board Swarm A during a period of fifteen months.

The need to analyze the scaling properties of N_e fluctuations according to different IMF orientations derives from the strong dependence of the high-latitude ionosphere electro-dynamics on the interconnection between the geomagnetic field and the IMF due to the occurrence of magnetic reconnection at the magnetopause. In fact, the high-latitude ionospheric convection pattern strongly depends on the interplanetary medium conditions, generating a two-cell plasma convection pattern that evolves as a function of the orientation of the IMF. As reconstructed using many years of data collected by different instruments installed on the ground or on satellites, balloons and rockets, the large-scale motion of ionospheric plasma changes considerably when B_z is southward or northward. When B_z is southward the plasma crosses the polar cap in the antisunward direction and then flows sunward at lower latitudes toward dawn and dusk, and forming a two-cells pattern (Cousins and Shepherd, 2010). Also the sign and strength of IMF B_y component is important for the location of these two cells. Indeed when B_y is positive, the plasma flows sunward from the dusk side, crosses local noon in the auroral zone and successively flows antisunward. When B_z is northward, reconnection processes are thought to take place tailward of the ionospheric cusp, giving rise again to a two-cell pattern, symmetric with respect to the noon-midnight direction, but with convection flow reversed with respect to the case of southward B_z, i.e. sunward at higher latitudes and antisunward at lower latitudes; moreover the two cells are smaller with respect to the southward B_z case, and mostly confined within the polar cap. Conversely, when B_y is negative the plasma flows sunward from the dawn side, crosses local noon and successively flows antisunward.

The role of large-scale ionospheric convection patterns is discussed in relation to the observed patterns of electron density and its scaling features. The paper is organized as follows. In Sections 2 and 3 we describe the dataset used and the analysis performed, respectively; in Section 4 we show and discuss the obtained results; in Section 5 we drive conclusions and highlight the future perspectives.

2. Data description

In this study, we use in situ electron density observations collected by Swarm A satellite. In detail, we analyze measurements recorded with 1 Hz resolution by the Langmuir probe of the Electric Field Instrument (EFI) (Knudsen et al., 2017) from April 1, 2014 to June 30, 2015. These data, which are Swarm Level 1b data, can be downloaded from the ESA ftp repository (ftp://swarm-diss.eo.esa.int). The time series has been carefully checked and the dubious values have been excluded

considering the information coming from the quality flags. Since the electron density properties are characterized by a solar-activity dependence we consider only measurements recorded during the maximum of solar cycle 24 so as to have a quasi-constant solar radio flux index ($F10.7$) (Tapping, 2013) guaranteed. Indeed, during the selected period $F10.7$ is equal to 140 ± 30 sfu, as shown in Fig. 1.

Maps of the average polar electron density are then drawn arranging data in quasi-dipole (QD) latitude and magnetic local time (MLT). The QD coordinate system is based on magnetic apex coordinates introduced by Richmond (1995) and, as suggested by the author, it is to be preferred to other reference frames when investigating *"phenomena related to horizontally stratified ionospheric currents"*. To display data with respect to the Sun position, MLT is used instead of QD-longitude. Being interested in the study of the dependence of electron density distribution on different IMF orientations in the *Y-Z* plane, we consider also 1-min IMF B_y and B_z measurements in the geocentric solar magnetic (GSM) reference system. These data are available on the OMNI website (www.cdaweb.gsfc.nasa.gov/istp-public/) and have been considered over the same time interval covered by Swarm data (April 1, 2014–June 30, 2015). However, because the ionosphere does not respond to fast changes of the IMF conditions (typically changes on timescales shorter than 20–30 min), in order to minimize the effects of such changes when classifying the data according to the different IMF orientations in the *Y-Z* plane, we filter them out using a moving average over a window of 30 min (Moen et al., 2015; Spicher et al., 2017).

The filtered IMF B_y and B_z components are used to identify four IMF angular sectors based on the value of IMF clock angle $\theta_c \in [0, 2\pi]$ that is defined as follows:

$$\theta_c = \begin{cases} \tan^{-1}\dfrac{B_y}{B_z} & \text{for } B_z \geq 0, B_y \geq 0, \\ \tan^{-1}\dfrac{B_y}{B_z} + 2\pi & \text{for } B_z > 0, B_y < 0, \\ \tan^{-1}\dfrac{B_y}{B_z} + \pi & \text{for } B_z < 0. \end{cases} \quad (1)$$

Based on the values of θ_c we define four IMF sectors with a width of $\pi/4$:

- Sector I: IMF–Northward for $\theta_c \in]\frac{15}{8}\pi, 2\pi\Big[\cup \Big[0, \frac{1}{8}\pi\Big]$ (i.e. $B_y \simeq 0$, $B_z > 0$);
- Sector II: IMF–Eastward for $\theta_c \in]\frac{3}{8}\pi, \frac{5}{8}\pi\Big]$ (i.e. $B_y > 0$, $B_z \simeq 0$);
- Sector III: IMF–Southward for $\theta_c \in]\frac{7}{8}\pi, \frac{9}{8}\pi\Big]$ (i.e. $B_y \simeq 0$, $B_z < 0$);
- Sector IV: IMF–Westward for $\theta_c \in]\frac{11}{8}\pi, \frac{13}{8}\pi\Big]$ (i.e. $B_y < 0$, $B_z \simeq 0$).

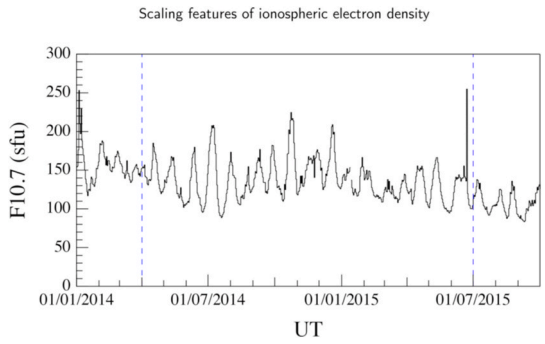

Fig. 1. The $F10.7$ solar index for the selected period from April 1, 2014 to June 30, 2015. The dashed vertical bars individuate the selected period. (1 sfu = 10^{-22} W m^{-2} Hz^{-1}).

To associate measurements made at ionospheric altitudes to the IMF measurements propagated at the bow shock available in OMNI database, a time delay of $\sim$ 30 min is considered. This time delay follows from an investigation made using delayed mutual information (DMI) as defined in Alberti et al. (2017). As external signals we have used the coupling functions ε_{PA} and ε_W proposed by Perreault and Akasofu (1978) and Wang et al. (2014), respectively, and the solar wind dynamic pressure p_{SW}. As a proxy for the magnetospheric response we have used *AE*, SYM-*H* and ASY-*H* indices. The effective delays obtained by estimating DMI between all possible couples of external signals and magnetospheric response proxies have then been averaged resulting in an average effective delay of 29 ± 6 minutes.

Fig. 2 displays polar maps of the average electron density in a QD-latitude (λ_{QD}) and MLT frame, for the four IMF sectors defined above. Maps refer to the Northern Hemisphere ($\lambda_{QD} > 50°$N) and reveal several of the most important and well-known features of electron density for the high-latitude ionosphere. Among these we mention that dayside electron density values are almost twice than those on the night side, as a consequence of the strong solar ionization which is the main source of free electrons in the ionosphere. This feature is always present, independently of the different IMF orientations.

Another feature is the region characterized by high electron density values which can be observed in the postnoon mid-latitude and sub-auroral ionospheric region. This is an ionospheric electron density feature visible during enhanced geomagnetic activity periods named, for this reason, storm-enhanced density (SED). Both ground-based and space observations have permitted to hypothesize its generation and decay mechanisms (e.g., Zou et al., 2014). Fig. 2 shows that SED region forms a plume that expands into the polar cap from the dayside along the streamlines of convection, producing the well known tongue-of-ionization (TOI), which has been suggested to be the projection in the ionosphere of the magnetospheric equatorial plume by Foster et al. (2002). The spatial distribution of the TOI in the polar cap region is clearly controlled by the IMF orientation depending both on B_y and B_z. In detail, TOI moves dawnward (duskward) with positive (negative) IMF B_y, respectively. Differently, for negative IMF B_z the TOI is narrower but more intense over the polar cap than for positive values. This feature is well in agreement with the role that IMF B_z and B_y components have on the polar ion convection pattern: B_z controls the cross polar cap potential and ion convection pattern while B_y the dawn-dusk asymmetry of this convection. A last feature concerns the sub-auroral ionospheric region where, primarily in the nightside, electron density shows a depletion which identifies the main ionospheric trough (MIT) separating the auroral and mid-latitude regions (Rodger et al., 1992). This is a very dynamic structure that represents the signature of the magnetospheric plasmapause in the nighttime ionosphere and it seems to change according to IMF orientation, moving equatorward and increasing its extension duskward, especially for negative IMF B_z.

3. Method of analysis

One of the fingerprints of turbulent fluctuations is the occurrence of scale-invariance and, in particular, of self-affinity of the velocity field fluctuations. The investigation of such a property can be done by analyzing the scaling features of the q^{th}-order moments of the velocity field increments (i.e. differences of velocity, typically along the flow direction) as proposed by Kolmogorov in 1941 (Kolmogorov, 1941a, b). This is done by computing the q^{th}-order structure functions, $S_q(\delta)$, defined as follows:

$$S_q(\delta) = \langle \left(v_{||}\left(\mathbf{r} + \delta\widehat{e}_{||}\right) - v_{||}(\mathbf{r}) \right)^q \rangle \sim \delta^{\gamma(q)} \quad (2)$$

where $\langle\rangle$ denotes the average, $\mathbf{r}$ is the position vector, δ is the spatial scale under investigation, $v_{||}(\mathbf{r})$ and $\widehat{e}_{||}$ are the velocity component parallel to the flow direction and the corresponding unit vector, respec-

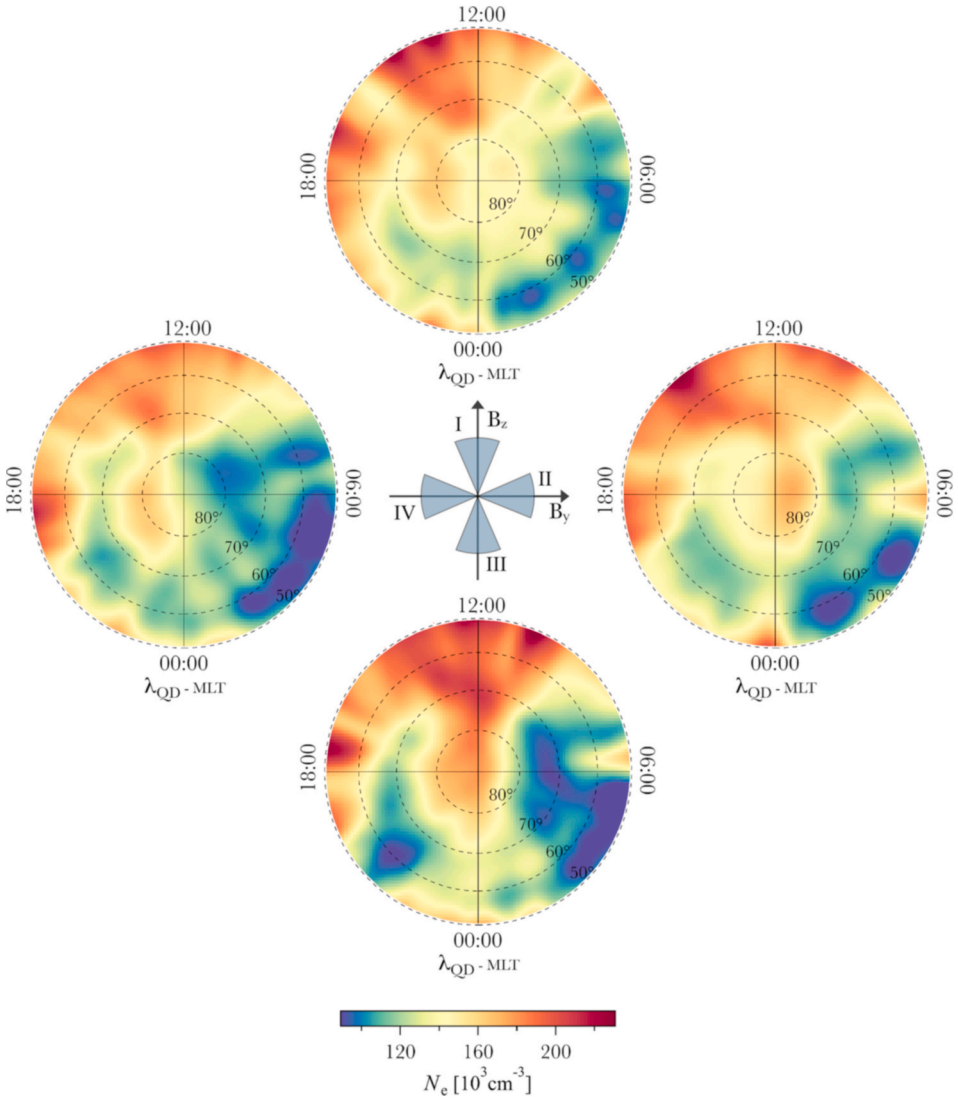

Fig. 2. Electron density maps. Polar view of the average spatial distribution of the electron density (N_e) for the Northern Hemisphere, in a QD-latitude ($\lambda_{QD} > 50°N$) and MLT reference frame, for four different IMF sectors shown in the center of the figure (blue areas indicate the circular sectors containing the considered clock angles). Maps have been drawn using data recorded on-board Swarm A from April 1, 2014 to June 30, 2015 and hence refer to an average altitude of $\sim$ 460 km. Dashed circles indicates (λ_{QD}=50°, 60°, 70° and 80°N)and (λ_{QD}> 50°N)..

tively, $\gamma(q)$ is a scaling exponent which is a function of the moment order q.

The above expression of the structure function can be generalized to investigate the scaling features of a signal $x(t)$ as follows:

$$S_q(\tau) = \langle |x(t+\tau) - x(t)|^q \rangle \sim \tau^{\gamma(q)} \quad , \tag{3}$$

where τ is the time delay that, in the case of an Eulerian point of view, can be read as the spatial scale of interest, assuming that the transit time of the structure under observation is faster than its evolution time. This assumption is the well-known Taylor's hypothesis (Taylor, 1938) which is generally assumed to be valid when analyzing turbulent flows with an Eulerian observational approach.

Each scaling exponent $\gamma(q)$ provides a different information on the features of the signal under investigation. In particular, the first scaling exponent $\gamma(1)$ is a measure of the self-affinity of the analyzed signal and is related to the persistent character of the signal increments. This scaling index, when confined in the range of $[0, 1]$ is generally analogous to the well-known Hurst exponent (H) (Hurst, 1956), so in what follows we will refer without distinction to either $\gamma(1)$ or H. More in general, being a measure of the self-affine nature of the signal, $\gamma(1)$ is also known as the Hölder exponent h. H can be interpreted as the long-term memory of the time series. Indeed it provides a measure of the tendency of $x(t)$ to either strongly move towards the mean or to cluster in a direction. When H takes values in the range $]0.5, 1[$ we say that $x(t)$ has a persistent behavior and we expect that a given fluctuation will be probably followed by another one of the same sign. In this case $x(t)$ tends to persist in a direction so that H will provide information on the memory time series and, consequently, on the dynamics of the system it represents. When H takes values in the range $]0, 0.5[$ we say that $x(t)$ has an antipersistent behavior and we expect that successive values will be characterized by fluctuations with alternating signs. Finally, $H = 0.5$ means that $x(t)$ is a completely uncorrelated time series as a Brownian random motion, $H = 0$ means that $x(t)$ describes the case of a white noise, $H = 1$ means that $x(t)$ is completely predictable, being a linear trend.

The second-order scaling exponent $\gamma(2)$, provides information on the scaling features of the autocorrelation function and is related, via the Wiener-Khinchin theorem (Wiener, 1964), to the spectral features of the signal under study. Indeed, a signal having a power spectral density (PSD) following a power law, namely $\sim f^{-\beta}$, is expected to be characterized by a second-order structure function $S_2(\tau)$ with the scaling exponent $\gamma(2) = \beta - 1$. Higher-order scaling exponents, $\gamma(q) \mid q \geq 3$, provide information on the scaling behavior of the tails of the probability density functions at large values of the signal increments.

The trend of the scaling exponents $\gamma(q)$ as a function of the moment-order q is expected to be linear, i.e. $\gamma(q) = kq$, in the case of simple affine (mono-fractal) signal, while for more complex signal displaying multi-affine (multifractal) properties $\gamma(q)$ is generally a convex function of q

(Frisch, 1995).

The evaluation of the local scaling exponent in a real signal, such as the time series obtained by the measurements made on-board of Swarm, requires some precautions. Indeed, the satellite along its orbit crosses regions characterized by different physical situations changing in space and time. Thus, in real signals/time series, the scaling features can show a local dependence on time and space. To overcome this issue we need to apply methods capable of extracting scaling features on a local basis. Here, we adopt a local structure function method, the so called Detrended Structure Function Analysis (DSFA) (De Michelis et al., 2015).

According to this method, the q^{th}-order structure function defined in Equation (3) is evaluated on a moving window of N points (seconds in our case being of 1 s the resolution of the analyzed time series). The width of the moving window must be at least 10^{q_m} points, being q_m the maximum moment order of the structure function. Once set the width of the moving window, here a linear trend is removed from the original time series to eliminate possible large-scale variations that can affect a correct estimation of the scaling features. Then, τ is let vary between given values of $\tau_{\min}$ and $\tau_{\max}$ so to estimate $S_q(\tau)$. Once known $S_q(\tau)$, $\gamma(q)$ can be evaluated for the given window associating its value with the central point of the window. The window is then moved forward by one point and the procedure described above repeated to cover the entire time series under investigation. In our case the smallest scale $\tau_{\min}$ that is possible to investigate is of 1 s, corresponding with the time resolution of the time series. The maximum time scale $\tau_{\max}$ depends on the number of points of the moving window. To have a statistically robust computation of the q^{th}-order scaling exponents we have to evaluate the corresponding q^{th}-order structure functions (S_q) on a moving window with a width of the order of $N \sim 10\tau$. So, we considered a moving window of $N = 301$ points (seconds), that allows us to robustly evaluate the first- and second- order structure functions up to $\tau_{\max} = 40$ s. Since the observed low-frequency fluctuations are mainly the effect of Doppler-shifted spatial variations (see e.g., Basu et al., 1990; De Michelis et al., 2016; 2020b), and since the orbital velocity of Swarm satellite is $\sim$ 7.6 km/s, this range of temporal scales allows us to analyze the features of the electron density fluctuations in the spatial scales between 8 and 300 km, and consequently to analyze some features of the electron density fluctuations that occur at the meso-scale.

4. Results and discussion

The application of DSFA to our data set, as described in Section 3, produced a 15-month long time series of the first- and second- order scaling exponents. Data have been then selected according to the value of the IMF clock angle, grouped into the four IMF sectors defined in Section 2 and translated into polar maps for the Northern Hemisphere.

Fig. 3 displays maps obtained for the first-order scaling exponent

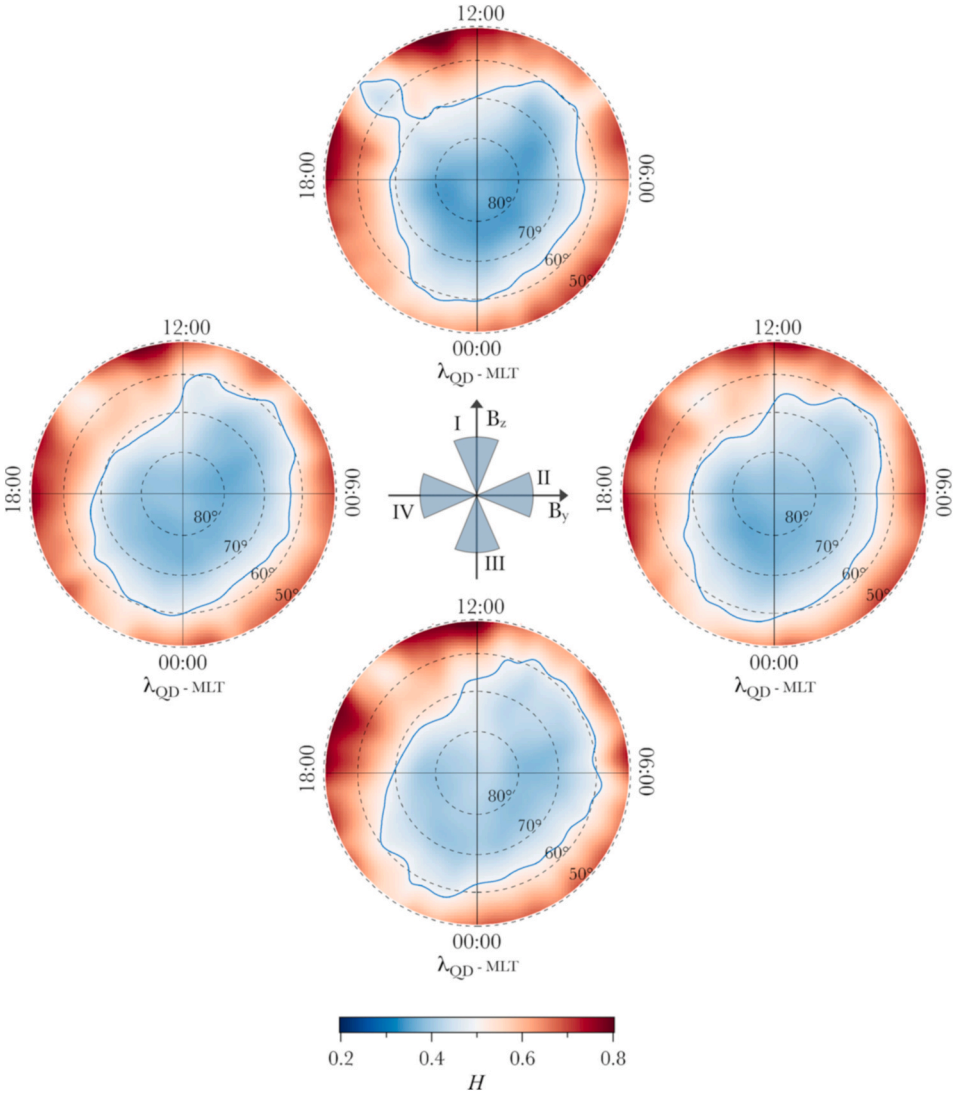

Fig. 3. First-order scaling exponent maps. Polar view of the first-order scaling exponent (Hurst exponent H) for the Northern Hemisphere, in a QD-latitude ($\lambda_{QD} > 50°$N) and MLT reference frame, for four different IMF sectors shown in the center of figure (blue areas indicate the circular sectors containing the considered clock angles). The blue line drawn in each map represents the isoline corresponding to $H = 0.5$. Maps have been drawn using data recorded on-board Swarm A from April 1, 2014 to June 30, 2015 and hence refer to an average altitude of $\sim$ 460 km. Dashed circles indicates $\lambda_{QD} = 50°$, 60°, 70° and 80° N.

(Hurst exponent). These maps reveal different features of N_e fluctuations which depend mainly on QD-latitude, MLT and to a lesser extent on IMF orientation. Fig. 3 suggests a persistent behavior ($H > 0.5$) of N_e fluctuations at mid latitudes and an antipersistent ($H < 0.5$) one at high latitudes. These two areas are those external and internal to the auroral oval. Inside the auroral oval, N_e fluctuations are characterized by an antipersistent behavior, which means a tendency for fluctuations to oscillate around an average value. Conversely, outside the auroral oval N_e fluctuations have a persistent character, that means the tendency of the fluctuations to cluster along a direction that can be increasing or decreasing. So, maps shown in Fig. 3 provide the important information that the different processes occurring inside and outside the auroral oval deeply influence the features of electron density fluctuations making them persistent and with a long correlation only outside the auroral region.

The transition between the two different behaviors of N_e fluctuations, occurring at $H = 0.5$, seems to be only partially controlled by IMF orientation. When IMF B_z component is positive, and hence the magnetosphere is in a closed configuration, the region characterized by an antipersistent behavior of N_e fluctuations tends to expand equatorwards on the dayside. To better appreciate the slight dependence of the transition zone between persistent/antipersistent behavior on IMF orientation, Fig. 4 displays a comparison among four different isolines corresponding to the value $H = 0.5$ of the Hurst exponent, obtained for each of the four IMF sectors and also shown in Fig. 3. Also in this case isolines are in a QD-latitude and MLT reference frame. It is known that during disturbed periods, which are associated with an open configuration of the magnetosphere, in the postnoon mid-latitude and sub-auroral ionospheric region we can observe a strong enhancement of the electron density (e.g., Foster et al., 2005; Liu et al., 2016; Zou et al., 2014). The different pattern that characterizes the isolines corresponding to the value $H = 0.5$ in first IMF sector, i.e. corresponding to values of IMF B_z that are always positive, could be interpreted in terms of the absence of this enhancement, which manifests on the scaling properties of the electron density fluctuations and in particular on their persistent or antipersistent character.

Fig. 5 displays polar view maps of the second-order scaling exponent $\gamma(2)$ associated with N_e fluctuations according to the selected IMF sectors. These maps show that N_e fluctuations are characterized by different scaling features depending on QD-latitude, MLT and IMF orientation. A peculiar feature of the second-order scaling exponent is that different values of $\gamma(2)$ are associated with different polar regions. In detail the polar cap region, where the electron density fluctuations have an antipersistent behavior, are characterized by $\gamma(2) \sim 0.66$. This implies, as explained in Section 3, electron density fluctuations with power spectral density characterized by a spectral exponent $\beta \sim 5/3$. However, some changes of the spectral exponent in this region can be observed as a function of the IMF orientation. In particular, in the TOI, which extends toward the polar cap region for southward IMF condition, the spectral exponent is slightly higher being $\sim 1.7 - 1.8$. This could be an effect of intermittency corrections that tend to increase the slope of the spectral density. We underline that electron density can behave as a passive scalar quantity (as recently underlined in Consolini et al. (2020a) for which a higher degree of intermittency is expected. Conversely, N_e fluctuations in the auroral regions are characterized by a spectral exponent $\beta \sim 1.7 - 2.0$. The observed spectral slope is quite well in agreement with the one of magnetic field fluctuations at frequencies below 1 Hz (Consolini et al., 2020b) for the magnetic field components perpendicular and parallel to the main geomagnetic field. This spectral slope again could be due to intermittent turbulence, generated by the particle precipitation and the features of FACs in this region as sketched in Consolini et al. (2020b). However, we cannot exclude that also stochastic fluctuations in the particle precipitation in this region could explain the observed spectral features. The observed spectral average features, as evaluated using the second-order scaling exponent $\gamma(2)$, are in the same range of values found by Kivanç and Heelis (1998) in their statistical study of ion density features in the high-latitude Northern ionosphere using DE2 satellite observations. There is, indeed, a statistical consistency inside standard errors between our spectral exponents and theirs (Kivanç and Heelis, 1998) if we average their values on the different seasons and compare them with our average values for the same regions (cusp, post-midnight, pre-midnight and polar cap as defined in Table 2 of Kivanç and Heelis (1998)). However, we remark that the occurrence of some differences between our results and those by Kivanç and Heelis (1998) could be a consequence of the different altitudes between DE2 and Swarm satellites, being the observations of Swarm done at a quasi constant altitude of approximately 450 km and those of DE2 made at altitudes ranging from 300 km to 1000 km. Lastly, the regions outside the auroral oval, that display a persistent character of the electron density fluctuations, have a spectral exponent $\beta \sim 2.3$. This steeper spectral slope could be due to a weak turbulence regime such as electrostatic drift wave turbulence in low-β plasmas, which shows spectral exponents in the range between -2 and -3 at low frequencies (Pecseli et al., 1983; Pécseli, 2015). These three classes of β values, besides the dependence on QD-latitude and MLT, display also a clear dependence on IMF orientation.

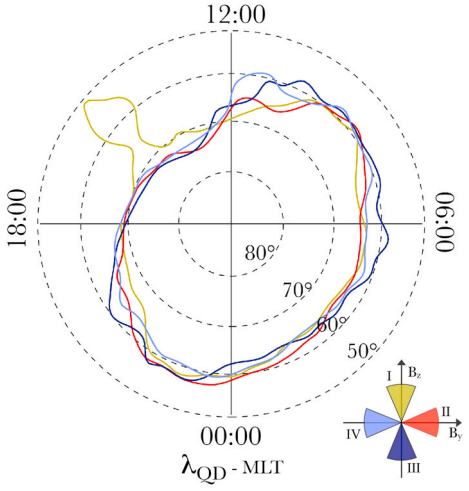

Fig. 4. First-order scaling exponents isolines. Comparison among the isolines (the same shown in Fig. 3) corresponding to the Hurst exponent $H = 0.5$ obtained for the four IMF sectors. A different color is associated to each sector as indicated in the bottom rightside of the figure. These isolines are displayed for the Northern Hemisphere in a QD-latitude ($\lambda_{QD} > 50°$N) and MLT reference frame. Dashed circles indicates $\lambda_{QD} = 50°$, 60°, 70° and 80° N.

The most striking result that emerges from the analysis of the spectral indices in the polar regions, is the peculiar shape of the high-latitude region where the spectral index is near 5/3 ($\beta = \gamma(2) + 1$). Indeed, the shell shape of the outer border of this region reminds of the shape of the plasmasphere boundary (plasmapause) (see, e.g., Goldstein and Sandel, 2005; Del Corpo et al., 2019), which is generally eroded in the dusk-noon sector during disturbed periods. To a first approximation we can imagine the plasmapause as a boundary which separates a dense and corotating plasma from a less dense but more transported plasma. However, plasmapause is not a single boundary but an interchange region characterized by a strong dynamics. For this reason, it is more correct to define it as a plasmasphere boundary layer. Here, processes of variability and instability naturally arise due to a continuous overlapping of plasma with different properties having origin in the equatorial plane of the inner magnetosphere or produced by the Sun. The particular nature of this region seems to be reflected in the scaling properties of the N_e fluctuations at high-mid latitudes of the ionosphere where the charged particles moving along magnetic field lines can strike it. Indeed, at high latitudes the magnetic field lines are connected either to the magnetosheath and solar wind, or far down just inside the magnetotail. This is a very interesting result, which paves the way to a better

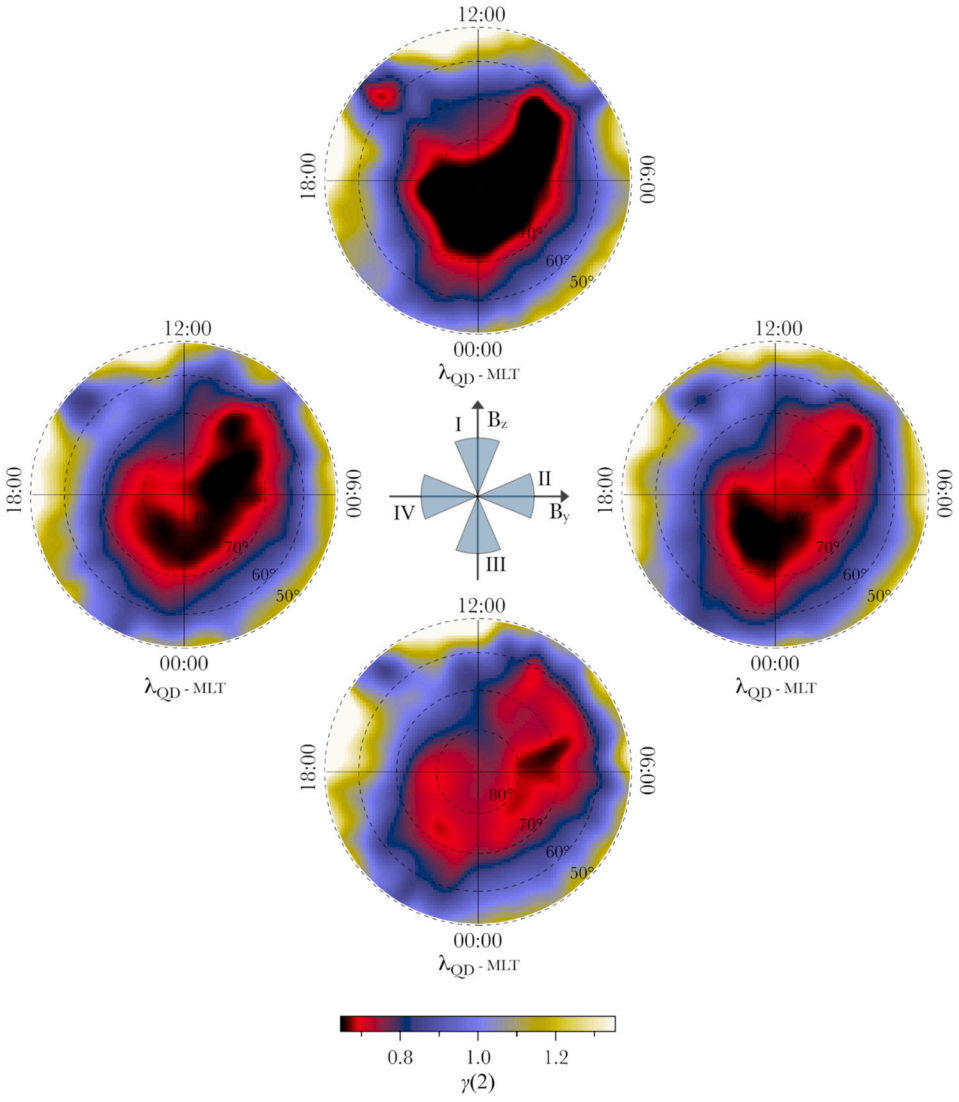

Fig. 5. Second-order scaling exponent maps. Polar view of the second-order scaling exponent ($\gamma(2)$) for the Northern Hemisphere, in a QD-latitude ($\lambda_{QD} > 50°$N) and MLT reference frame, for four different IMF sectors shown in the center of figure (blue areas indicate the circular sectors containing the considered clock angles). Maps have been drawn using data recorded on-board Swarm A from April 1, 2014 to June 30, 2015 and hence refer to an average altitude of $\sim$ 460 km. Dashed circles indicates $\lambda_{QD} = 50°$, 60°, 70° and 80° N.

comprehension of some processes due to the magnetosphere ionosphere coupling.

We finish our analysis by evaluating the intermittency of the electron density fluctuations. Intermittency is a peculiar property of turbulence being a measure of the complexity and inhomogeneity of the cascade mechanism and of the dissipation field at the smallest scales. In other words, intermittency is due to an uneven distribution of the dissipation in the velocity field, which is conversely localized in a subset of it. On the side of the mathematical characterization, intermittency manifests in what is called anomalous scaling and/or multifractality of the quantity under investigation. The term anomalous scaling refers to the fact that there is not a linear dependence of the structure function scaling exponents on the order q. As a consequence of this anomalous scaling it is possible to introduce an intermittency index (I) capable of measuring the deviation from linearity of the relation between $\gamma(q)$ and q using the two exponents $\gamma(1)$ and $\gamma(2)$. This quantity is defined as $I = 2\gamma(1) - \gamma(2)$ and it is expected to be $I > 0$ where the intermittency phenomenon occurs. Fig. 6 displays polar view maps of the intermittency of N_e fluctuations grouped according to the selected IMF sectors. These polar maps reveal that the highest values of intermittency can be found at mid latitudes where they seem to follow approximately the same shape of the plasmasphere boundary in proximity of the low-latitude boundary of the auroral oval. Thus, regions in the ionosphere corresponding to the plasmasphere are characterized by electron density fluctuations with a level of intermittency higher than the others.

Several different processes can be at the origin of the observed features of N_e fluctuations. Indeed, inside the auroral oval, electron density perturbations can be due to various mechanisms, including particle precipitation and ionization, heating and cooling of ionospheric density, transport as well as chemical reactions. The particle precipitation pattern itself is due to a combination of discrete and diffuse auroral precipitations, which are both highly variable processes. This variability and complexity could be at the base of the stochastic nature of the ionospheric density revealed in our analysis and reported in Fig. 6. However, our finding seems to be well in agreement with previous results suggesting the occurrence of turbulence in the high-latitude ionospheric regions. These regions are, indeed, characterized by plasma density fluctuations and structures that result in irregularities produced by different mechanisms that operate at different spatial scales. The origin of these irregularities, which is very complex, can be partially associated also with a turbulence phenomenon, often linked to the occurrence of instabilities.

Among the most important ones we mention the $\mathbf{E} \times \mathbf{B}$ gradient drift, the current-convective and Kelvin-Helmholtz instabilities. Spectral features of N_e fluctuations can provide information on the different nature of the ionospheric turbulence due to the quasi-passive scalar nature of electron density. Indeed, fluctuations of passive scalar quantities are directly driven by those of the velocity field. Thus, the occurrence of a

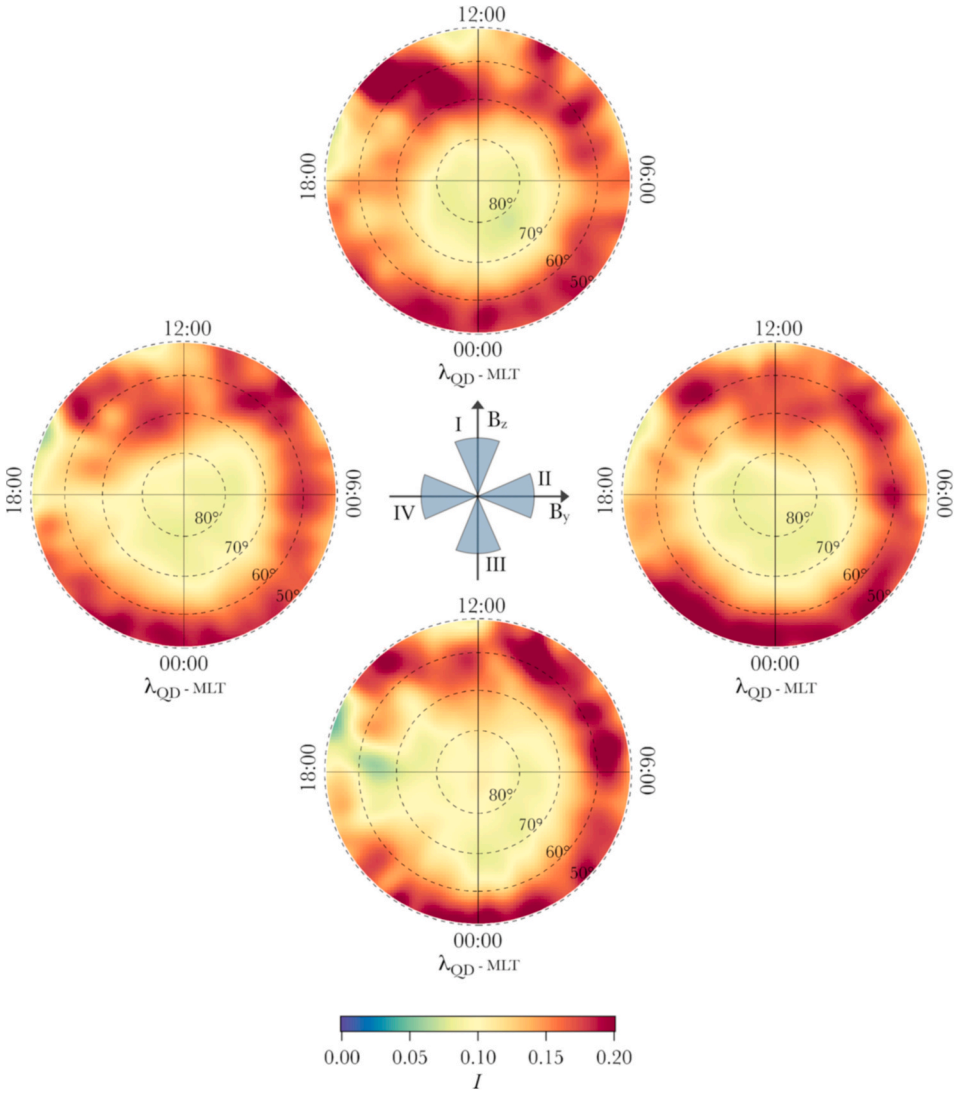

Fig. 6. Intermittency maps. Polar view of intermittency (I) for the Northern Hemisphere, in a QD-latitude ($\lambda_{QD} > 50°$N) and MLT reference frame, for four different IMF sectors shown in the center of figure (blue areas indicate the circular sectors containing the considered clock angles). Maps have been drawn using data recorded onboard Swarm A from April 1, 2014 to June 30, 2015 and hence refer to an average altitude of ∼ 460 km. Dashed circles indicates $\lambda_{QD} = 50°$, 60°, 70° and 80° N.

power spectral density with a slope $\beta \sim 5/3$ in the case of N_e fluctuations, observed mainly in the polar cap region, can be a consequence of the occurrence of turbulent processes. These could be ascribed to gradient drift and current-convective instabilities in the case of a direct cascade process, or to a Kelvin-Helmholtz instability in the case of an inverse cascade (Kintner and Seyler, 1985). These instabilities can both directly and indirectly generate plasma density fluctuations in a large range of scales, from several hundred of kilometers to meters. These plasma density fluctuations may give rise to irregularities of gradually smaller scale sizes, giving rise to a cascade process typical of turbulence phenomena. The Kelvin-Helmholtz and/or $\mathbf{E} \times \mathbf{B}$ gradient drift origin of the observed turbulence are the most likely ones and worthy of further investigations, being the polar cap region the one where the high-latitude convection cells are located and thus, where strong shear flows can occur.

5. Summary and conclusions

Data recorded by instruments on-board one of the Swarm satellites during a time interval of 15 months (April 2014–June 2015) offered us the opportunity to analyze how the average patterns of ionospheric electron density, of its scaling features and intermittency vary at latitudes between 50°N and 90°N according to different IMF orientations. The obtained average spatial distributions of N_e, $\gamma(1)$, $\gamma(2)$ and I can play a role in increasing the knowledge of the physical processes at the base of the coupling in the solar wind-magnetosphere-ionosphere system and in developing ionospheric models capable of reproducing those turbulence phenomena that characterize the high-latitude ionosphere. Indeed, at the present time, models of the ionosphere currently used by the scientific community do not consider turbulence processes despite these have been proved to play an important role in the ionospheric dynamics (Dyrud et al., 2008; Pécseli, 2016; Grach et al., 2016; De Michelis et al., 2017).

We have seen that, as expected, the distribution of the electron density in the λ_{QD} – MLT plane is clearly modulated by the IMF, while the scaling properties of its fluctuations do not always show such a clear dependence on IMF orientation. This clearly emerges from Fig. 4 where it is not possible to appreciate the expected dependence of the auroral oval extension on IMF orientation, i.e. on an open or closed configuration of the magnetosphere. However, a first interesting result is provided by the maps of the Hurst exponent, shown in Fig. 3. These maps provide the important information that the different processes occurring inside and outside the auroral oval deeply influence the features of electron density fluctuations making them persistent and with a long correlation only outside the auroral region.

A second result worth being underlined concerns the case of the second-order scaling exponent whose maps are shown in Fig. 5. These maps reveal that electron density fluctuations are characterized by

values of $\gamma(2) \sim 0.66$ inside the auroral oval, by slightly higher value along the boundary of the auroral oval, and even higher values equatorward the auroral oval. Inside the auroral oval, there are areas where N_e fluctuations show an antipersistent character and contemporaneously a power spectral density with a spectral exponent $\beta \sim 5/3$. We can then suppose that turbulent processes could be responsible for this peculiar feature of N_e fluctuations.

A third interesting result relates to the possible use of the second-order scaling exponent to investigate some processes occurring at the plasmapause.

The approach here proposed could be considered as an example of the new insights that a complete understanding of the electron density features on the IMF would provide in the modeling of the effects of solar wind impact on the magnetosphere-ionosphere coupling and in the framework of Space-Weather studies. This work is a first step in this direction with a special emphasis to the role that scaling features and turbulence might play.

Declaration of competing interest

The authors declare that they have no known competing financial interests or personal relationships that could have appeared to influence the work reported in this paper.

Acknowledgments

The results presented rely on data collected by one of the three satellites of the Swarm constellation. We thank the European Space Agency (ESA) that supports the Swarm mission. Swarm data can be accessed at http://earth.esa.int/swarm. The authors kindly acknowledge V. Papitashvili and J. King at the National Space Science Data Center of the Goddard Space Flight Center for the use permission of 1 min OMNI data and the NASA CDAWeb team for making these data freely available. The authors acknowledge financial support from European Space Agency (ESA contract N. 4000125663/18/I-NB- "EO Science for Society Permanently Open Call for Proposals EOEP-5 BLOCK4" (INTENS)) and the Italian National Program for Antarctic Research under contract N. PNRA18_00289-SPIRiT. G. C. and G. B. have benefitted from discussions within the International Space Science Institute (ISEE) Team # 455 "Complex Systems Perspectives Pertaining to the Research of the Near-Earth Electromagnetic Environment".

References

Alberti, T., Consolini, G., Lepreti, F., Laurenza A., M. Vecchio, Carbone, V., 2017. Timescale separation in the solar wind-magnetosphere coupling during St. Patrick's day storms in 2013 and 2015. J. Geophys. Res. Space Phys. 122, 4266–4283.

Basu, S., Basu, S., MacKenzie, E., Coley, W.R., Hanson, W.B., Lin, C.S., 1984. F region electron density irregularity spectra near auroral acceleration and shear regions. J. Geophys. Res. Space Phys. 89, 5554–5564.

Basu, S., Basu, S., MacKenzie, E., Coley, W.R., Sharber, J.R., Hoegy, W.R., 1990. Plasma structuring by the gradient drift instability at high-latitudes and comparison with velocity shear driven processes. J. Geophys. Res. Space Phys. 95, 7799–8295.

Basu, S., Basu, S., MacKenzie, E., Fougere, P.F., Coley, W.R., Maynard, N.C., Winningham, J.D., Sugiura, M., Hanson, W.B., Hoegy, W.R., 1988. Simultaneous density and electric field fluctuation spectra associated with velocity shears in the auroral oval. J. Geophys. Res. Space Phys. 93, 115–136.

Consolini, G., De Michelis, P., Alberti, T., Coco, I., Giannattasio, F., Tozzi, R., Carbone, V., 2020a. Intermittency and passive scalar nature of electron density fluctuations in the high-latitude ionosphere at Swarm altitude. Geophys. Res. Lett. 47, e2020GL089628 https://doi.org/10.1029/2020GL089628.

Consolini, G., De Michelis, P., Alberti, T., Giannattasio, F., Coco, I., Tozzi, R., Chang, T.T. S., 2020b. On the multifractal features of low-frequency magnetic field fluctuations in the field-aligned current ionospheric polar regions: Swarm observations. J. Geophys. Res. 125, e27429 https://doi.org/10.1029/2019JA027429.

Cousins, E.D.P., Shepherd, S.G., 2010. A dynamical model of high-latitude convection derived from SuperDARN plasma drift measurements. J. Geophys. Res. Space Phys. 115, A12329. https://doi.org/10.1029/2010JA016017.

Cowley, S.W.H., 1982. The causes of convection in the Earth's magnetosphere: a review of developments during the IMS. Rev. Geophys. 20, 531–565.

De Michelis, P., Consolini, G., Tozzi, R., 2015. Magnetic field fluctuation features at Swarm's altitude: a fractal approach. Geophys. Res. Lett. 42, 3100–3105.

De Michelis, P., Consolini, G., Tozzi, R., Marcucci, M.F., 2016. Observations of high-latitude geomagnetic field fluctuations during St.Patrick's Day storm: swarm and SuperDARN measurements. Earth Planets Space 68.

De Michelis, P., Consolini, G., Tozzi, R., Marcucci, M.F., 2017. Scaling features of high-latitude geomagnetic field fluctuations at Swarm altitude: impact of IMF orientation. J. Geophys. Res. Space Phys. 122, 10548–10562.

De Michelis, P., Consolini, G., Tozzi, R., Giannattasio, F., Quattrociocchi, V., Coco, I., 2019. Features of magnetic field fluctuations in the ionosphere at Swarm altitude. Ann. Geophys. 62, 1–11.

De Michelis, P., Pignalberi, A., Consolini, G., Coco, I., Tozzi, R., Pezzopane, M., Giannattasio, F., Balasis, G., 2020. On the 2015 St. Patrick's storm turbulent state of the ionosphere: hints from the swarm mission. J. Geophys. Res. 125, e27934 https://doi.org/10.1029/2020JA027934.

Del Corpo, A., Vellante, M., Heilig, B., Pietropaolo, E., Reda, J., Lichtenberger, J., 2019. Observing the cold plasma in the Earth's magnetosphere with the EMMA network. Ann. Geophys. 62, 1–19.

Dungey, J.W., 1961. Interplanetary magnetic field and the auroral zones. Phys. Rev. Lett. 6, 47–48.

Dyrud, L., Krane, B., Oppenheim, M., Pécseli, H.L., Trulsen, J., Wernik, A.W., 2008. Structure functions and intermittency in ionospheric plasma turbulence. Nonlinear Process Geophys. 15, 847–862.

Earle, G.D., Kelley, M.C., Ganguli, G., 1989. Large velocity shears and associated electrostatic waves and turbulence in the auroral F region. J. Geophys. Res. Space Phys. 94, 15321–15333.

Foster, J.C., Coster, A.J., Erickson, P.J., Holt, J.M., Lind, F.D., Rideout, W., McCready, M., van Eyken, A., Barnes, R.J., Greenwald, R.A., Rich, F.J., 2005. Multiradar observations of the polar tongue of ionization. J. Geophys. Res. Space Phys. 110 https://doi.org/10.1029/2004JA010928.

Foster, J.C., Erickson, P.J., Coster, A.J., Goldstein, J., Rich, F.J., 2002. Ionospheric signatures of plasmaspheric tails. Geophys. Res. Lett. 29 https://doi.org/10.1029/2002GL015067, 1–1–1–4.

Friis-Christensen, E., Lühr, H., Hulot, G., 2006. Swarm: a constellation to study the Earth's magnetic field. Earth Planets Space 58, 351–358.

Friis-Christensen, E., Lühr, H., Knudsen, D., Haagmans, R., 2008. Swarm - an Earth observation mission investigating geospace. Adv. Space Res. 41, 210–216.

Frisch, U., 1995. Turbulence: the Legacy of A. N. Kolmogorov. Cambridge University Press.

Giannattasio, F., De Michelis, P., Consolini, G., Quattrociocchi, V., Coco, I., Tozzi, R., 2019. Characterising the electron density fluctuations in the high-latitude ionosphere at Swarm altitude in response to the geomagnetic activity. Ann. Geophys. 62, 1–14.

Goldstein, J., Sandel, B.R., 2005. The Global Pattern of Evolution of Plasmaspheric Drainage Plumes, vol. 159. Washington DC American Geophysical Union Geophysical Monograph Series, p. 1. https://doi.org/10.1029/159GM02.

Grach, S., Sergeev, E., Mishin, E., Shindin, A.V., 2016. Dynamic properties of ionospheric plasma turbulence driven by high-power high-frequency radiowaves. Uspekhi Fizicheskih Nauk 186, 1189–1228.

Heppner, J.P., Maynard, N.C., 1987. Empirical high-latitude electric field models. J. Geophys. Res. Space Phys. 92, 4467–4489.

Hurst, H.E., 1956. Methods of using long-term storage in reservoirs. Proc. ICE 5, 519–543.

Iyemori, T., Nakanishi, K., Aoyama, T., Yokoyama, Y., Koyama, Y., Lühr, H., 2015. Confirmation of existence of the small-scale field-aligned currents in middle and low latitudes and an estimate of time scale of their temporal variation. Geophys. Res. Lett. 42, 22–28.

Jin, Y., Spicher, A., Xiong, C., Clausen, L.B.N., Kervalishvili, G., Stolle, C., 2019. The status of observations and theory of high latitude ionospheric and magnetospheric plasma turbulence. J. Geophys. Res. Space Phys. 124, 1262–1282.

Kintner, P.M., Seyler, C.E., 1985. The status of observations and theory of high latitude ionospheric and magnetospheric plasma turbulence. Space Sci. Rev. 41, 1572–9672.

Kivanç, Ö., Heelis, R.A., 1998. Spatial distribution of ionospheric plasma and field structures in the high-latitude F region. J. Geophys. Res. 103, 6955–6968. https://doi.org/10.1029/97JA03237.

Knudsen, D.J., Burchill, J.K., Berg, K., Cameron, T., Enno, G.A., Marcellus, C.G., King, E. P., Wevers, I., King, R.A., 2003. A low-energy charged particle distribution imager with a compact sensor for space applications. Rev. Sci. Instrum. 74, 202–211.

Knudsen, D.J., Burchill, J.K., Buchert, S.C., Eriksson, A.I., Gill, R., Wahlund, J.E., Ahlen, L., Smith, M., Moffat, B., 2017. Thermal ion imagers and Langmuir probes in the Swarm electric field instruments. J. Geophys. Res. Space Phys. 122, 2655–2673.

Kolmogorov, A., 1941a. The local structure of turbulence in incompressible viscous fluid for very large Reynolds' numbers. Akademiia Nauk SSSR Doklady 30, 301–305.

Kolmogorov, A.N., 1941b. Dissipation of energy in locally isotropic turbulence. Akademiia Nauk SSSR Doklady 32, 16.

Liu, J., Wang, W., Burns, A., Oppenheim, M., Dimant, Y., 2018. Faster traveling atmosphere disturbances caused by polar ionosphere turbulence heating. J. Geophys. Res. Space Phys. 123, 2181–2191.

Liu, J., Wang, W., Burns, A., Yue, X., Zhang, S., Zhang, Y., Huang, C., 2016. Profiles of ionospheric storm-enhanced density during the 17 march 2015 great storm. J. Geophys. Res. Space Phys. 121, 727–744. https://doi.org/10.1002/2015JA021832.

Materassi, M., Forte, B., Coster, A., Skone, S. (Eds.), 2020. The Dynamical Ionosphere. Elsevier.

Moen, J., Hosokawa, K., Gulbrandsen, N., Clausen, L.B.N., 2015. On the symmetry of ionospheric polar cap patch exits around magnetic midnight. J. Geophys. Res. 120, 7785–7797. https://doi.org/10.1002/2014JA020914.

Pécseli, H., 2016. Low Frequency Waves and Turbulence in Magnetized Laboratory Plasmas and in the Ionosphere. 2053–2563. IOP Publishing.
Pécseli, H.L., 2015. Spectral properties of electrostatic drift wave turbulence in the laboratory and the ionosphere. Ann. Geophys. 33, 875–900. https://doi.org/10.5194/angeo-33-875-2015.
Pecseli, H.L., Mikkelsen, T., Larsen, S.E., 1983. Drift wave turbulence in low-β plasmas. Plasma Phys. 25, 1173–1197. https://doi.org/10.1088/0032-1028/25/11/001.
Perreault, P., Akasofu, S.I., 1978. A study of geomagnetic storms. Geophys. J. Roy. Astron. Soc. 54, 547–573.
Richmond, A.D., 1995. Ionospheric electrodynamics using magnetic apex coordinates. J. Geomagn. Geoelectr. 47, 191–212.
Rodger, A.S., Moffett, R.J., Quegan, S., 1992. The role of ion drift in the formation of ionisation troughs in the mid- and high-latitude ionosphere-a review. J. Atmos. Terr. Phys. 54, 1–30.
Ruohoniemi, J.M., Greenwald, R.A., 1996. Statistical patterns of high-latitude convection obtained from Goose Bay HF radar observations. J. Geophys. Res. Space Phys. 101, 21743–21764. https://doi.org/10.1029/96JA01584.
Spicher, A., Clausen, L.B.N., Miloch, W.J., Lofstad, V., Jin, Y., Moen, J.I., 2017. Interhemispheric study of polar cap patch occurrence based on Swarm in situ data. J. Geophys. Res. 122, 3837–3851. https://doi.org/10.1002/2016JA023750.
Spicher, A., Miloch, W.J., Clausen, L.B.N., Moen, J.I., 2015. Plasma turbulence and coherent structures in the polar cap observed by the ICI-2 sounding rocket. J. Geophys. Res. Space Phys. 120, 10959–10978.
Tapping, K.F., 2013. The 10.7 cm solar radio flux (F10.7). Space Weather 11, 394–406. https://doi.org/10.1002/swe.20064.
Taylor, G.I., 1938. The spectrum of turbulence. P. Roy. Soc. A Math. Phy. 164, 476–490.
Vasyliūnas, V.M., Song, P., 2005. Meaning of ionospheric Joule heating. J. Geophys. Res. Space Phys. 110 https://doi.org/10.1029/2004JA010615. A02301.
Wang, C., Han, J.P., Li, H., Peng, Z., Richardson, J.D., 2014. Solar wind-magnetosphere energy coupling function fitting: results from a global MHD simulation. J. Geophys. Res. Space Phys. 119, 6199–6212.
Weimer, D.R., 2005. Improved ionospheric electrodynamic models and application to calculating Joule heating rates. J. Geophys. Res. Space Phys. 110, A05306. https://doi.org/10.1029/2004JA010884.
Wiener, N., 1964. Time Series. M.I.T. Press, Cambridge, Massachusetts, p. 42.
Yin, F., Lühr, H., Park, J., Wang, L., 2019. Comprehensive analysis of the magnetic signatures of small-scale traveling ionospheric disturbances, as observed by Swarm. J. Geophys. Res. Space Phys. 124, 10794–10815.
Zou, S., Moldwin, M.B., Ridley, A.J., Nicolls, M.J., Coster, A.J., Thomas, E.G., Ruohoniemi, J.M., 2014. On the generation/decay of the storm-enhanced density plumes: role of the convection flow and field-aligned ion flow. J. Geophys. Res. Space Phys. 119, 8543–8559. https://doi.org/10.1002/2014JA020408.